Electrical Resistivity Reconstruction of Graphite Moderator Bricks From Multi-Frequency Measurements and Artificial Neural Networks

DOI:
10.1109/JSEN.2021.3080127

Document Version
Accepted author manuscript

Electrical Resistivity Reconstruction of Graphite Moderator Bricks from Multi-Frequency Measurements and Artificial Neural Networks

HenokTesfalem, Joel Hampton, Adam D Fletcher, Matthew Brown and Anthony J Peyton

***Abstract*—This paper discusses an artificial neural inversion approach for non-destructive testing of the graphite moderator bricks that make up the cores of Advanced Gas-Cooled Reactors (AGR). The study employed fully connected feedforward neural networks consisting of four hidden layers and trained with backpropagation approach using Levenberg-Marquardt optimisation algorithm. The approach is based on multi-frequency (MF) eddy current (EC) measurements, and combinations of simulated and measured datasets from a laboratory sample and one of the operating reactor core, along with different regularisation parameters were used to train and test the networks. Various types of artificially generated errors were added to the data during training procedures, which in turn allowed for error tolerance and improved the generalisation of the ANNs to unseen test datasets. First, the ANN was tested using unseen simulated data, followed by the measurements collected from laboratory sample and one of the operating reactor core. The first test from the unseen simulated data showed mean profile error ranging between 1.30% and 8.20%, whereas the profiles estimated from reactor core measurements showed mean profile error ranging between 1.84% and 17.80% when compared with the resistivity measurements from trepanned graphite sample taken out of the reactor core. Further comparison of the network outputs against the profiles estimated using traditional iterative inversion algorithm indicates reasonable agreement between the two approaches with the exception of one case, but the solution time for the ANN was found to be over three orders of magnitude faster than the iterative inversion algorithm.**

***Index Terms*—Graphite, Eddy Currents, Artificial Neural Networks, Resistivity Profile, Multi-frequency, Non-Destructive Testing**

I. Introduction

The work in this paper aims to address an inspection problem relating to the civil nuclear industry. The civil nuclear reactors are built with significant complexity to achieve robust strictures, sustain the required chemical reaction, and most of all to meet the standards set out by the regulatory authorities. Due to these complex strictures and hostile environments within the cores of the civil nuclear reactors it is often challenging to assess the condition of the inner core structures even after the reactors are shutdown.

Graphite is one of the materials used as a core component within some of reactor designs, particularly in Advanced Gas-Cooled Reactors (AGR). The graphite core in an AGR design serves to moderate the fast-moving neutrons, facilitate thermal energy transfer to the coolant gas and maintain the lattice spacing between the fuel assemblies and control rods [1]. The parts of the graphite bricks in the AGR, which are in direct proximity to the fuel elements, are subject to the highest radiation flux. As a result, they suffer most from irradiation and radiolytic oxidation [2]-[3].

Radiolytic oxidation of the fuel channel bricks is mainly caused by decomposition of the carbon dioxide coolant into carbon monoxide and oxidizing species when exposed to gamma radiation, which then react with the graphite structure to increase the size of porosity, and hence leads to a reduction in graphite density or "weight loss" [2]-[3]. Consequently, oxidation could affect the core structural integrity margins and neutron moderating ability, and potentially reduce the operating lifetime of the reactor. The fuel channel bricks in the reactor core are not able to be replaced; therefore, the normal operation and safety functions of the AGRs depend significantly upon the condition of these bricks. For this reason, the assessment of AGR graphite properties is important to support the safety case for continued operation of the reactors.

Due to the conducting nature of the graphite, eddy current (EC) based non-destructive testing (NDT) has been used in the past to characterise its internal properties, particularly as the graphite density can be closely correlated with electrical resistivity [4], [5], hence giving insight into its strength and neutron moderating ability.

EC-based NDT is very well established, and its use within the civil nuclear industry is increasing significantly in recent years [5]. One of the driving factors for the use of EC-NDT in the nuclear industry is its simplicity and robustness when deployed in radioactive environments, such as the core of an AGR. However, the amount of information that can be obtained from an EC system is limited if operated at a single frequency [6]. To overcome this limitation, multi-frequency (MF) excitation can be applied to excite the EC sensor. In this way full spectral information about the material of interest can be obtained [7]- [12]. In this context, with the application of the MF excitation technique, it is possible to probe the graphite fuel channel brick to different depths and collect

HenokTesfalem, Joel Hampton, Adam D Fletcher and Anthony J Peyton are with Department of Electrical and Electronic Engineering, University of Manchester, M13 9PL, UK.Matthew Brown is with EDF-Energy, Barnett Way, Barnwood, Gloucester, GL4 3RS, UK.

The work presented in this paper is funded by the UK Engineering and Physical Science Research Council and EDF Energy under grant number EPSRC/University of Manchester grant number IAA 212.

enough data to characterise its electrical properties through its wall thickness.

However, one of the major challenges of material characterisation with EC measurements (particularly depth profiling) is that the measured data depends upon many factors including the material structure, sensor configuration, magnetic and electrical properties of the material under test. Assuming an optimised sensor configuration, non-magnetic material with unknown electrical properties (which is the case for the problem considered in this paper), complex material structures still pose difficulties for depth profiling. This is because the field distribution within complex structures are affected by the geometry of the object and requires robust inversion algorithms. Significant progress has been made concerning inverse EC problem theory, and it has been applied to several areas, including [8]-[15]. One of the first non-uniform conductivity profiling and crack shape reconstruction approach was proposed by Norton et al [8], [9]. In [9] the authors presented a detailed theory of inverse EC methods for conductivity and crack shape reconstruction using forward and adjoint method to calculate the Jacobian matrix and used iterative least square algorithm for reconstruction. The work in [8] employed an iterative nonlinear least square approach to reconstruct radially varying conductivity profiles demonstrating the ability of the proposed method to recover the unknown electrical conductivity from MF EC measurements. The unknown electrical conductivity reconstruction was made by minimising the discrepancies between the computed impedance from the forward model and measured data in a least square sense. Another inverse EC approach was proposed by Bowler et al [10]. In this work the authors proposed a method based on MF EC measurements and steepest descent algorithm to reconstruct the conductivity distributions and thickness of layered structure independently. Related work describing a method for estimating the thickness and conductivity of layer conductors by comparing the measured data with Dodd and Deeds [16] theoretical solution was presented by Moulder et al [11] and Uzal et al [12]. Yin et al [13], [14], [15] proposed analytical solution for solving forward problem for air cored coil placed above layered conductor and employed a modified Newton Rapson method to reconstruct both smoothly varying and step changing electrical conductivity and magnetic permeability profiles of a sample as a function of depth. Although these works lay the foundations for inverse EC problems, these methods are usually computationally expensive when solving large and complex problems, and applications are therefore limited to post-measurement processing.

Another model based inversion approach to reconstruct the reactor brick conductivity/resistivity profiles were studied by [17], [18], [19], [20], [21]. These studies have demonstrated the practical feasibility of the iterative inversion approach for reconstructing the properties of the graphite moderator brick from MF EC measurements however, as before they are limited to post measurement processing.

One of the major limitations of these approaches is that they all tend to be computationally expensive, and could not be used for real time reconstruction of the graphite moderator brick properties, unless significant simplifications are made on the reconstruction procedures, which could compromise the accuracy of the solution.

A direct conductivity measurement such as four-point potential drop techniques [22] and the MF EC measurement phase response [23] has been used in the past to measure the resistivity of a conducting material and the porosity of metal foams. However, these approaches are only limited to bulk conductivity measurements, and electrical contacts also have practical problems for deployment in reactor core as the approach in [22] requires attaching the probe to the sample.

A computationally efficient inverse EC method for reconstructing defect shapes within conducting material was reported by Tamburrino et al [24]. In this approach the authors used monotonicity imaging method avoiding the need to solve the inverse problem iteratively, hence increasing the speed by which the inverse solution is attained. Further modification of this approach could allow efficient way of reconstructing the resistivity profiles as a function of depth. However, the problem considered in this paper involved complex structure with relatively smooth radial resistivity variation within cylindrical moderator brick that has $\approx 100\,mm$ through-wall thickness. In addition, the presence of methane holes and key-way slots within the graphite bricks may pose additional difficulties when adopting the above approach.

An approach based on an artificial neural network (ANN) has the potential for depth profiling, and have been employed by many researchers for NDT applications, particularly for material defect identification, classification and characterization of conducting and composite materials [25] [26], [27], [28], [29]. A well-trained ANN is capable of mapping non-linear relationships between the measured responses and defects within the material of interest, whilst improving the solution speed by a significant amount.

In this paper, we extend our studies in [21] with the aim of increasing the reconstruction speed by employing an artificial neural inversion to estimate the reactor brick resistivity profile from MF EC data. A simple feedforward neural network consisting of four-hidden layers was used for this study. The ANN was trained using a backpropagation approach along with a Levenberg-Marquardt optimisation algorithm. We used combinations of simulated and measured datasets to train, test and validate the ANNs. The test procedures of the trained ANN models first started with a simplified case using unseen simulated data. This was then followed by tests using the MF EC experimental data from laboratory samples and the measurements collected from one of operating reactor core. The estimated profiles from neural inversions were then compared with the solution from an iterative inversion and the measurements from trepanned graphite sample taken out of the reactor core.

II. BACKGROUND

A. Measurement system and operational principle

EC based NDT exploits the principle of electromagnetic induction. A coil carrying an alternating current generates a time-harmonic primary field around the coil that induces closed-loop eddy currents flowing inside a conducting material placed within the field. The induced ECs in turn generate a secondary field, which can be detected by a pick-up

coil. Small changes in the electrical properties of the material of interest would alter the ECs flow, and hence the detected signal. Therefore, this information could be used to estimate the electrical properties of the material using appropriate signal and data processing techniques.

NDT of the graphite core in the AGRs is carried out from the brick bores using a specialized in-core inspection tool (Fig. 1). This tool is deployed from the top of the pile cap, and is fitted with gradiometer sensors equally separated circumferentially round the tool. The EC sensors in the tool are arranged to inspect the graphite brick over its radial cross section as well as to measure the density variation around the brick bore axially and circumferentially [5].

The tool has a rotating head enclosed by a cylindrical stainless steel casing, and uses non-conducting mechanical scissor-type arms to deploy the EC sensors towards the fuel channel bore. The inspections are made during outages of the reactors while the fuel elements are removed. During the inspection, the tool is lowered by a hoist into the bore of the fuel channel bricks using chains and an umbilical cable. The measurement speed, location and other inspection functions of the tool are set from a control console on the pile cap.

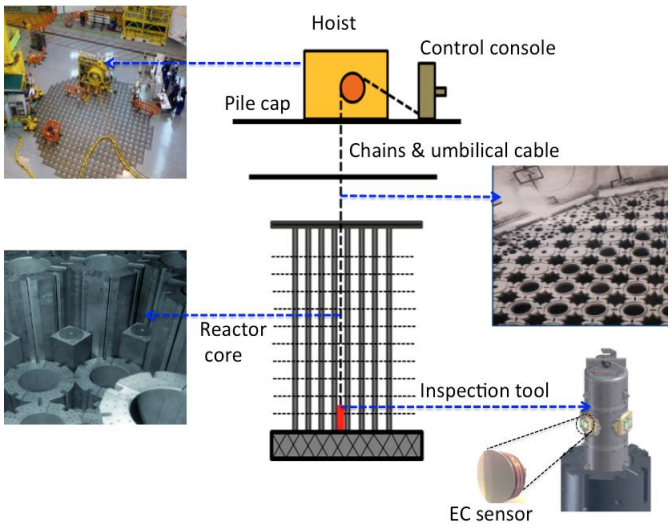

Fig. 1. Eddy current based AGR core inspection system along with illustration of the main core components and inspection procedures, Reproduced from [5].

B. *Artificial neural network*

Artificial Neural Networks (ANN) are simply mathematical models that generate functions to map the input data with a desired output target [32]. Although ANNs are being widely used for other applications such as image recognition and classification [33] [34], their use for NDT applications was limited until recent years, particularly for defect identification and characterization of conducting and composite materials [25], [26], [27], [28], [29], [31], [35], [36], [37]. ANNs are capable of mapping the non-linear relationships between the measured responses and defects within the material of interest. In addition, the solution time for ANNs, particularly for the problem considered in this paper are much faster than conventional iterative inversion methods, which may also mean that they could be used for real-time application. However, one of the main drawbacks of ANN is that they usually require large amount of training datasets covering many scenarios of a particular NDT problem, and tend to be application specific [29], [30], [38].

Although there are wide range of machine learning methods, they are normally categorised in to four groups: supervised learning, unsupervised learning, semi-supervised learning and reinforcement learning. The ANN approach considered in this paper lies within the supervised learning categories, meaning that the model learns when presented with an input and target datasets, and able to predict the output when presented with a new dataset.

One of the most commonly used type of ANNs is a feedforward neural network. In this type of neural network, the neurones are arranged in different layers connected to one another between the input and output layers through the weight and bias. The weights connected to each neurone determine the importance of the previous neurone input and usually updated during the training process until the optimum values are found. Activation functions (transfer functions) are used to pass the weighted sum of the neurones, this essentially means multiplying the weighted sum of the neurones with an activation function that determines the output value of the neurones. Mathematically, a simple single layer feedforward neural network can be described as follows. Given an input x_i, weight w_{ij} and bias b of a simple single layer feedforward neural network (where i is the index for the number of input neurones and ij is the associated weight between the input and the output layers), the ANN output can be represented as (1)

$$y_i = \sigma\left(\sum_i x_i w_{ij} + b\right) \tag{1}$$

where σ is the activation function that limits the output from reaching vary large value, and also introduce a non-linearity in this case.

There exist various activation functions that can be used within ANNs, each with their own distinct advantages for different applications. For the application considered in this paper, we decided to use a combinations of non-linear activation functions (hyperbolic tangent and sigmoid) in the hidden layers to allow the model to learn complex functions. The output layer activation function is chosen as a linear function because the problem considered here is regression problem.

For the hyperbolic tangent activation function the output (y_i) is given by (2), whereas for sigmoid and linear functions the output (y_i) is given as in (3) and (4) respectively.

$$y_i = \frac{2}{1+e^{(-2\sum_i x_i w_{ij} - b)}} - 1 \tag{2}$$

$$y_i = \frac{1}{1+e^{(-\sum_i x_i w_{ij} - b)}} \tag{3}$$

$$y_i = \sum_i x_i w_{ij} + b \tag{4}$$

The network weight (w_i) and bias (b) values are updated through the backpropagation training technique. A backpropagation training algorithm is a form of optimisation

algorithm that determines suitable weight and bias to minimise the errors e between the network outputs (y_i) and target values (t_i). To illustrate this, consider a Levenberg-Marquardt (LM) optimisation algorithm for updating the weights and bias of the ANN.

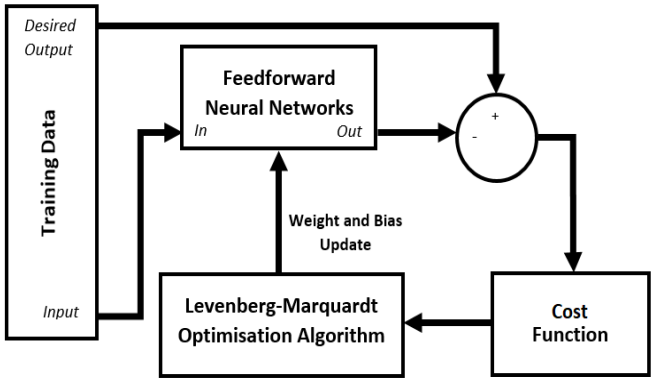

Fig. 2: Illustrations of the feedforward neural network with Levenberg-Marquardt backpropagation training algorithm.

Given the Jacobian $\mathbf{J}_k = \frac{\partial e_k}{\partial p_k}$, where e_k is the errors between the network output y_k and t_k at the kth iteration ($e_k = t_k - y_k$) , and the p_k is the weight (w_k) and bias (b_k) variables , the Gradient and the Hessian are given by (5) and (6) respectively.

$$\boldsymbol{G} = \mathbf{J}_k(p_k)^T e_k \tag{5}$$

$$\mathbf{H} \approx \mathbf{J}_k(p_k)^T \mathbf{J}_k(p_k) \tag{6}$$

It should be noted that the Hessian in (6) is approximated using the Gauss Newton method. The backpropagation training update is then given by (7).

$$p_{k+1} = p_k - (\mathbf{J}_k(p_k)^T \mathbf{J}_k(p_k) + \mu_k I)^{-1} \mathbf{J}_k(p_k)^T e_k \tag{7}$$

The cost function C of the feedforward ANN at n_{th} epoch is normally given by the squared sum of the errors between the network outputs and target values (8).

$$C_n = \frac{1}{N}\sum_i^N (t_i - y_i)^2 \tag{8}$$

here N is the number of complete training datasets that the network has seen.

To regularise the weights of individual neurons, the cost function can be further modified as (9)

$$C_n = \frac{1}{N}\sum_i^N (t_i - y_i)^2 - \frac{\lambda}{N}\sum_i^N (t_i - y_i)^2 + \frac{\lambda}{N}\sum_i^N (w_i)^2 \tag{9}$$

where λ is the regularisation parameter, a term that can be added to improve the generalisation of the network. It should be noted when $\lambda = 0$ the C_n in (9) is equal to (8). Fig. 2 shows a graphical illustrations of the feedforward neural network with a backpropagation training algorithm.

III. Methodology

A. Network architecture

As mentioned earlier, a simple feedforward ANN consisting four-hidden layers is used for this study. The first three hidden layers contain twenty-eight neurones, whereas the last hidden layer contains ten neurones. The four hidden-layers and the number of neurones stated here were selected based on trial and error test. Generally, the larger the number of neurones and hidden layers means the network will contain sufficient weights to allow it learn small features of the training data, and hence improve the non-linear mapping between the input and target datasets. However, there is also a trade-off between having large number of hidden layers or number of neurones and the time required for training. In other words, the larger the number of hidden layers and number of neurones the longer it takes to train and the more complex the network becomes. Another problem with large number of neurones and hidden layers is that the network could potentially memorise the training data resulting in overfitting. There exist several methods that could be used to reduce the overfitting of the network such as adding noise or errors in the training data, and applying regularisation to the network during the training procedures. For the problem considered in this paper combination of both regularisation approaches were used to improve network generalisation.

The input data consists of inductance spectra with fourteen frequency points ranging between 10 Hz and 4 kHz and arranged in a logarithmic scale with 5 points per decade, and output datasets are a conductivity vector with seven unknowns as illustrated in Fig.3. Three different types activation functions were used during the implementation of the ANN. Hyperbolic tangent activation function (2) for the neurones between the first and second hidden layers (HL1 and HL2 in Fig.3), whereas for the third (HL3) and fourth (HL4) hidden layers sigmoid (3) and linear activation function (4) were used. The hyperbolic tangent and sigmoid activation functions were mainly used to allow the model to learn complex functions. Extensive training experiments also shows that the combinations of hyperbolic tangent, sigmoid and linear

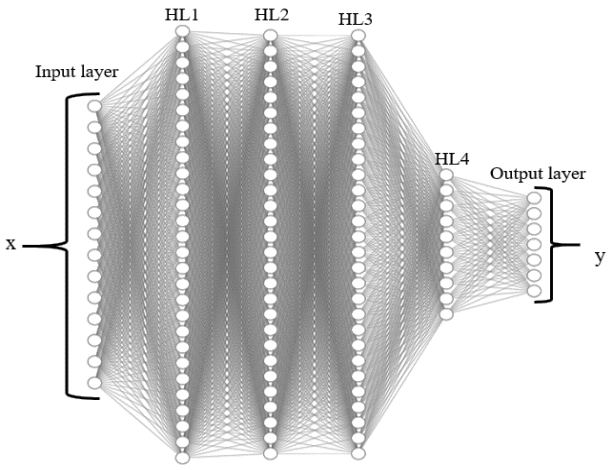

Fig. 3: Illustrations of the feedforward ANN employed for this study

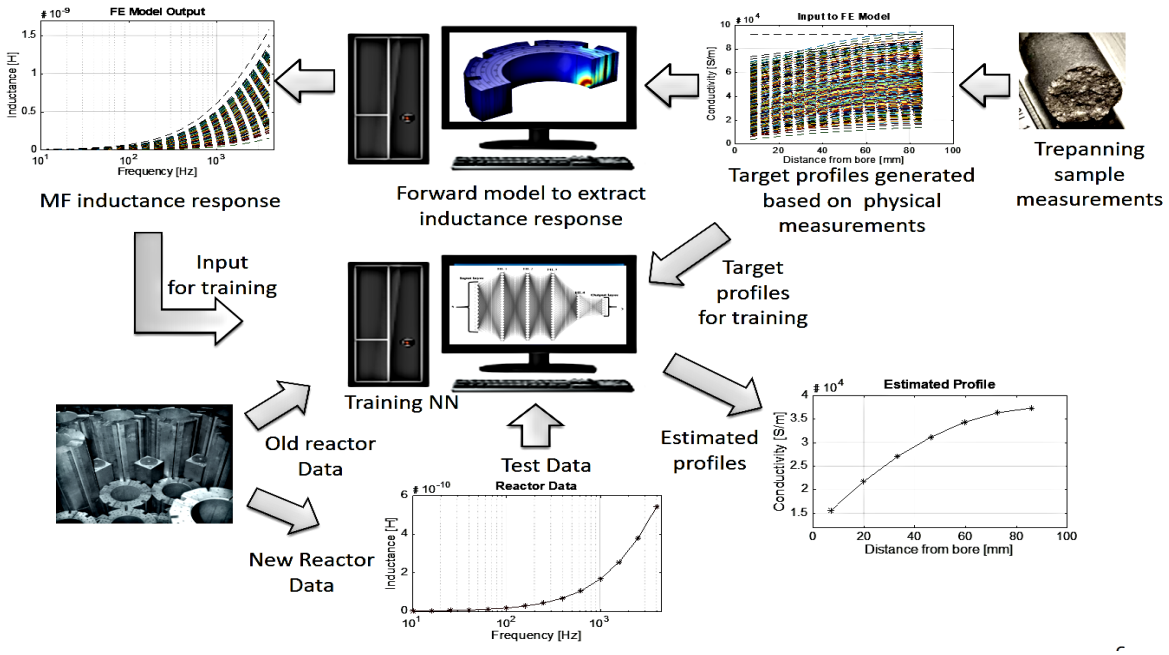

Fig. 4: Illustration of the training and testing procedures of the ANN trained to estimate the reactor bricks resistivity profiles as a function of depth from the bore

activation functions for the ANNs considered in this paper produced better performance than other cases.

The ANN was trained using a backpropagation training approach with a Levenberg-Marquardt (7) optimisation algorithm to update the weights of each neurone in every layer during the training procedure.

B. Forward modelling

One of the major challenges in machine learning and ANN for NDT applications is obtaining sufficient training datasets to allow the network to learn various scenarios of the inspection problem. In practice it is not always possible to obtain many experimental datasets for training the ANN, particularly for the problem considered in this paper. For this reason, a large amounts of training data were generated using a finite element forward model. The forward model was implemented such that it best represents the physical and electromagnetic properties of the fuel channel graphite brick and measurement system.

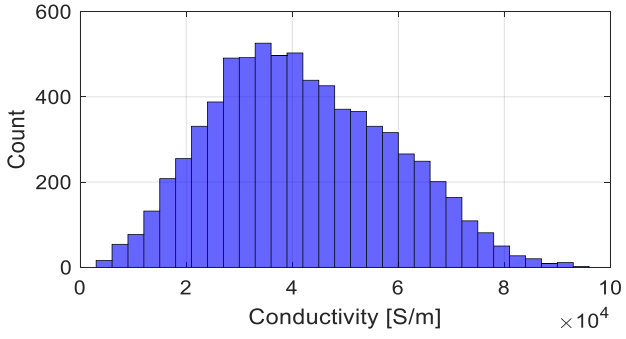

Fig. 5: Illustrations of the range of conductivity distributions of the samples used to generate inductance response

The forward model inputs were determined by initially gathering the resistivity profiles from some of the historically measured physical properties of fuel channel graphite bricks which covers over 100 profiles. The profiles were then extrapolated further based on the ranges of the known resistivity values to generate additional profiles and was used as an input to our forward model to obtain the corresponding inductance responses. In total we generated 1058 original datasets and these data was further extended by adding gaussian and smoothly varying errors making up a total of 10583 MF data. Fig.5 illustrates range of the conductivity distributions of the samples used to generate the inductance responses.

In addition, test sample were prepared, replicating a potential radial resistivity variations of the graphite fuel channel brick (Fig. 6) to train, test and validate the ANN. Further model calibration procedures were applied to the test datasets using the measurements from a graphite brick with known bulk electrical conductivity such that: $\boldsymbol{D}_{cal} = \boldsymbol{D}_{un} \times \left(\frac{\boldsymbol{D}_{\sigma_{bulk\_sim}}}{\boldsymbol{D}_{\sigma_{bulk\_mes}}}\right)$, where $\boldsymbol{D}_{cal}$ is the calibrated test data, $\boldsymbol{D}_{un}$ is the test data prior to calibration, $\boldsymbol{D}_{\sigma_{bulk\_sim}}$ is the simulated data from a model with known bulk electrical conductivity and $\boldsymbol{D}_{\sigma_{bulk\_mes}}$ is the measurement collected from a sample with identical bulk electrical conductivity. The full details of the implementation of the fuel channel brick forward model can be found in our previous work related to graphite moderator bricks [21].

C. Training datasets

Two different ANNs were trained to estimate the resistivity profiles of the laboratory sample and reactor bricks. The main reason for implementing two different ANNs is due to the

difference in brick geometries (such as key-way slots and methane holes) between the laboratory sample and reactor bricks, which could lead to different EC responses even if they have similarities in electrical properties. For this reason, two forward models were also implemented each replicating the physical and electromagnetic properties and the measurement systems of the reactor and laboratory bricks to extract datasets and to train the ANNs.

During the training of the ANN for reactor bricks, the simulated datasets were extracted from a forward model replicating historically measured physical and electromagnetic properties of the graphite bricks and the measurement system. The test datasets were directly measured from one of the operating reactor core at the locations where trepanning samples were extracted and measured. It should be noted that the trepanning sample is a cylindrical sample extracted from the reactor core with Ø=19 mm approximately 75 mm long, and measured in a laboratory condition.

To allow for error tolerance and improve the generalisation of the network to unseen test data we added two types of artificial errors into the input training datasets. The first type of error is randomly distributed gaussian noise with SNR of 40dB, 35dB and 30dB, whereas the second type is smoothly varying errors with the amplitudes ranging between of 0.5% and 3% of the mean MF inductance data. In both cases maintaining identical target profiles between the error-free and the data with added error such that $[D_{IN}\ (D_{IN}+\varepsilon)] \Rightarrow [D_T\ \ D_T]$ for the training and target datasets, where D_{IN} is the original simulated error-free training dataset, ε is the error added to the original training dataset and D_T is the target dataset. The total training dataset used for reactor ANN was 148162 data points or 10583 MF datasets. We used hold-out approach to split the data into 90 % of training and 10 % for validation and test set. Preliminary test results suggest that the network reasonably generalises to unseen datasets therefore, further cross validation of the model was not carried out.

In principle, the above method of generating training datasets allows the network to maintain some levels of error tolerance when tested with measured datasets. Fig. 4 illustrates the training and testing procedures of the ANN trained to estimate the reactor brick radial resistivity profile as a function of depth from the graphite bore.

The effect of the regularisation parameter (λ) on the ANN output was tested during the training procedure. The regularisation parameter was varied between λ=0 and $\lambda = 0.2$ for both the reactor and laboratory brick ANNs, whilst maintaining identical datasets and network structure. The variation of λ during the training process allowed us to select the parameter that gives the least error between the target and estimated profile during the training, validation and testing phase.

D. Testing

The preliminary test of the trained ANN was based on unseen simulated data. The unseen simulated data in this case refers to those extracted from the forward model, but that has not been used at any point to train, test or validate the network.

Secondly, measurements were collected from a laboratory sample, which replicated different weight-loss profiles across its radial thickness (see Fig. 6) to further test the trained ANN. The laboratory sample has a total height$\approx 900\ mm$ equivalent to those in a single layer of the actual reactor core. The entire 900 mm graphite brick was divided into four sections each with $180\,°$ radial span and 300 mm height. Two different patterns replicating different weight-loss scenarios were generated and a multi-frequency inductance response due to each pattern was measured.

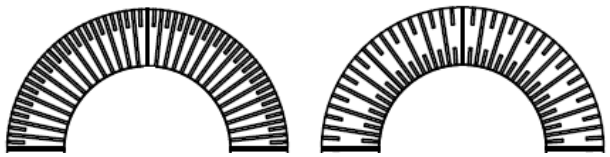

(a) (b)

Fig. 6: Cross-sectional illustrations of the different patterns of the laboratory sample brick used to replicate different density loss of an AGR brick. It should be noted that in reality each of the above 2D images represents semi-cylinder brick with 92 mm through-wall thickness and 300 mm height, and the lines represents the drilled hole patterns (Ø=4mm), which are created to represents different weight loss scenarios.

During the measurements in both laboratory and reactor conditions, we injected the exciter coil with a signal consisting of frequencies ranging between 10 Hz and 4 kHz with 5 point per decade in a logarithmic-scale, and measured the response due to the graphite being inspected. Further multi-frequency measurements from a brick with known bulk electrical conductivities were carried out. The measurements from the brick with known bulk electrical conductivity was mainly used to calibrate our model with the measurement system to compensate for any residual errors, and to test how well the ANN generalises to measured data.

Once the ANN was tested for the laboratory sample, the training procedure was extended to train and test the reactor brick ANN using the measurements collected from one of the operating AGR cores.

IV. RESULTS AND DISCUSSION

Fig. 7 and Table I show the test results from the unseen simulated dataset when using the ANN trained with different regularisation parameters. As can be seen in Table I the ANN estimated the unknown resistivity profiles with reasonable degree of accuracy with the error ranging between 1.30 % to 8.20 %. However, closer examination of the estimated profile errors reveals that the ANNs trained with $\lambda = 10^{-7}$and $\lambda = 10^{-5}$ produced the smallest error compared to other cases suggesting that the ANNs trained with these parameters should be used for estimating brick resistivity profiles from the reactor measurements.

Fig. 8 shows the estimated resistivity profiles of the laboratory graphite brick with different patterns of radial drilled holes. As mentioned in Section III.D the ANN for this particular laboratory sample was trained using different datasets extracted from another forward model created to replicate the drilled brick physical and electromagnetic

properties and the measurement system. As in the previous case different weight regularisation parameters were incorporated into the ANN to improve the generalisation of the network to unseen experimental data. As can be seen in Fig. 8, the ANNs trained with different regularisation parameters more or less reproduced the expected profile trends from the brick with two different radially drilled hole patterns. However, the exact resistivity profiles generated by each

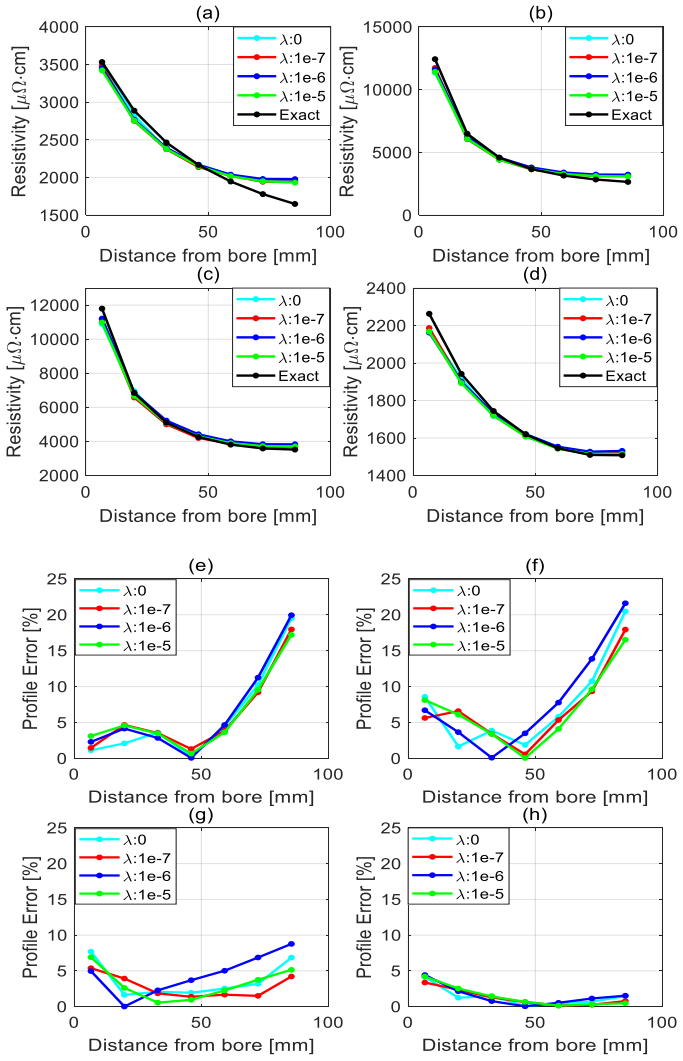

Fig. 7: Estimated verses exact profiles using simulated unseen datasets extracted from the one of the reactor brick model (a to d) and the corresponding errors related to each of the estimated profiles (e to h).

TABLE I
MEAN RESISTIVITY PROFILE ERRORS OF THE ESTIMATED SOLUTIONS IN FIG 6A TO 6D

Reg pram	Mean error for (a)	Mean error for (b)	Mean error for (c)	Mean error for (d)
$\lambda = 0$	5.90 %	7.57 %	3.70 %	1.37 %
$\lambda = 10^{-7}$	6.00 %	6.98 %	2.85 %	1.26 %
$\lambda = 10^{-6}$	6.46 %	8.17 %	2.52 %	1.51 %
$\lambda = 10^{-5}$	6.04 %	6.85 %	3.17%	1.39 %

drilled hole pattern is unknown at the moment due to difficulties in determining a bulk equivalent resistivity profile from a course pattern of drill holes. The only known resistivity profile is the bulk sample profile which is a homogeneous resistivity of 1075 $\mu\Omega.cm$ and the measurements from the this brick was used to calibrate the model data.

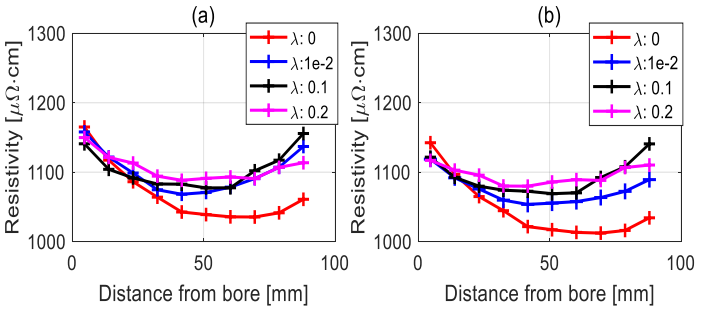

Fig. 8: Estimated resistivity profiles of the graphite brick consisting two different redial drilled hole patterns. Note the labels (a and b) in the above plots corresponds to the drilled patters shown in Fig. 6a and 6b.

For this reason, two different criteria have been used in order to allow us select a suitable regularisation parameter for the laboratory sample ANN. The first criterion is based on the estimated solution that gives the smallest error with respect to the homogeneous profile, that is the ANN that gives the least error when estimating the homogeneous profile will fulfil the first criteria. The second criterion is based on the drilled hole patterns, which are expected to be proportional to the resistivity profiles i.e. the closer the drilled holes the higher the resistivity value and vice versa. In addition, we used a Parallel model (10) volume fraction calculation method, (which was originally formulated to determine the effective properties of two-phase materials [39]) to estimate the resistivity of the brick with different drilled hole patterns and compare it with those estimated using the ANN.

$$\sigma_{eff} = (1 - f)\sigma_{bulk} + f\sigma_{hole} \tag{10}$$

where σ_{eff} is the effective conductivity of the brick, f is the volume fraction, σ_{bulk} is the conductivity of undrilled region and σ_{hole} is the conductivity of the drilled holes.

Fig. 9 and Fig. 10 show a flowchart of the optimum regularisation parameter selection procedure and the profile error with respect to homogeneous profile (1075 μΩ. cm)

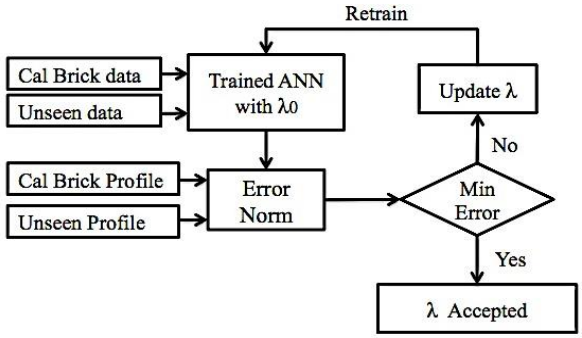

Fig. 9: A flowchart illustrating regularisation parameter selection criteria. Note: The Calibration brick data (Cal Brick data) and the unseen test data are independent datasets and the error norm from each is used to select suitable regularisation parameter for the ANN.

when estimated using the ANNs trained with different regularisation parameters (λ). Although the difference in the errors are not very significant, it is clear to see that the ANN trained with $\lambda = 0$ and $\lambda = 10^{-2}$give the smallest error.

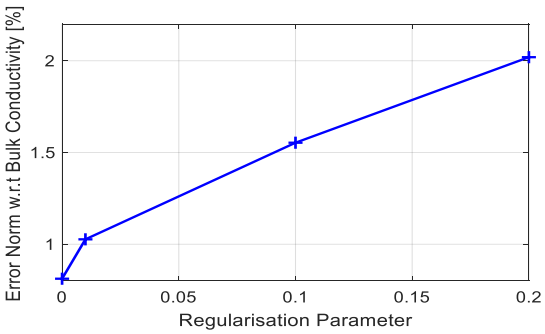

Fig. 10: Laboratory sample brick ANN regularisation parameter verses profile errors with respect to the brick with known bulk conductivity

In principle, the network should give near zero error as the measurement from a brick with known homogenous conductivity profile is already seen by the network. However, the addition different percentage errors on the training data means that the network has to compromise between the different training data that has identical target profiles, leading to small error on the estimated profiles. Similar results can also be seen in Table II (A) and (B) where the estimated bore and periphery conductivity values are shown along with the drilled holes spacing for each pattern. According to the radially drilled hole spacing in the brick bore and periphery (Table II) and the estimated profiles using different values of λ (Fig.8 and Fig. 10), the most representative profile trends was obtained when the ANN is trained with $\lambda = 0$ and $\lambda = 10^{-2}$. As λ increases beyond 10^{-2} the profile errors tend to increase. The reason that we see the smallest errors from the ANN trained with the two smallest regularisation parameters in this case $\lambda = 0$ and $\lambda = 10^{-2}$ could be that the errors added on the training data already acted to regularise the ANN, allowing for some level of error tolerance in the measured data, therefore adding higher value of λ resulted in additional regularisation being introduced during the training and hence

TABLE II

THE BORE AND PERIPHERY RESISTIVITY VALUES OF A GRAPHITE BRICK WITH TWO DIFFERENT HOLE PATTERNS (A AND B) WHEN ESTIMATED USING THE ANN TRAINED WITH $\lambda = 0$, $\lambda = 10^{-2}$,VOLUME FRACTION MODEL AND ITERATIVE INVERSION

Method	Pattern 1			
	Bore + 4.6 mm		Periphery - 4.6 mm	
	Hole distance (mm)	Value ($\mu\Omega.cm$)	Hole distance (mm)	Value ($\mu\Omega.cm$)
Post-Cal $\lambda = 0$	14.62	1165.00	11.67	1061.00
Post-Cal $\lambda = 10^{-2}$	14.62	1158.00	11.67	1137.00
Pre-Cal $\lambda = 0$	14.62	1116.00	11.67	1107.00
Pre-Cal $\lambda = 10^{-2}$	14.62	1152.00	11.67	991.90
Vol- fraction	14.62	1291.00	11.67	1363.00
Iterative-inv	14.62	1296.00	11.67	1344.00

(A)

Method	Pattern 2			
	Bore + 4.6 mm		Periphery - 4.6 mm	
	Hole distance (mm)	Value ($\mu\Omega.cm$)	Hole distance (mm)	Value ($\mu\Omega.cm$)
Post-Cal $\lambda = 0$	10.96	1142.00	17.51	1034.00
Post-Cal $\lambda = 10^{-2}$	10.96	1119.00	17.51	1089.00
Pre-Cal $\lambda = 0$	10.96	1101.00	17.51	1109.00
Pre-Cal $\lambda = 10^{-2}$	10.96	1113.00	17.51	1020.00
Vol- fraction	10.96	1379.00	17.51	1250.00
Iterative-inv	10.96	1466.00	17.51	1395.00

(B)

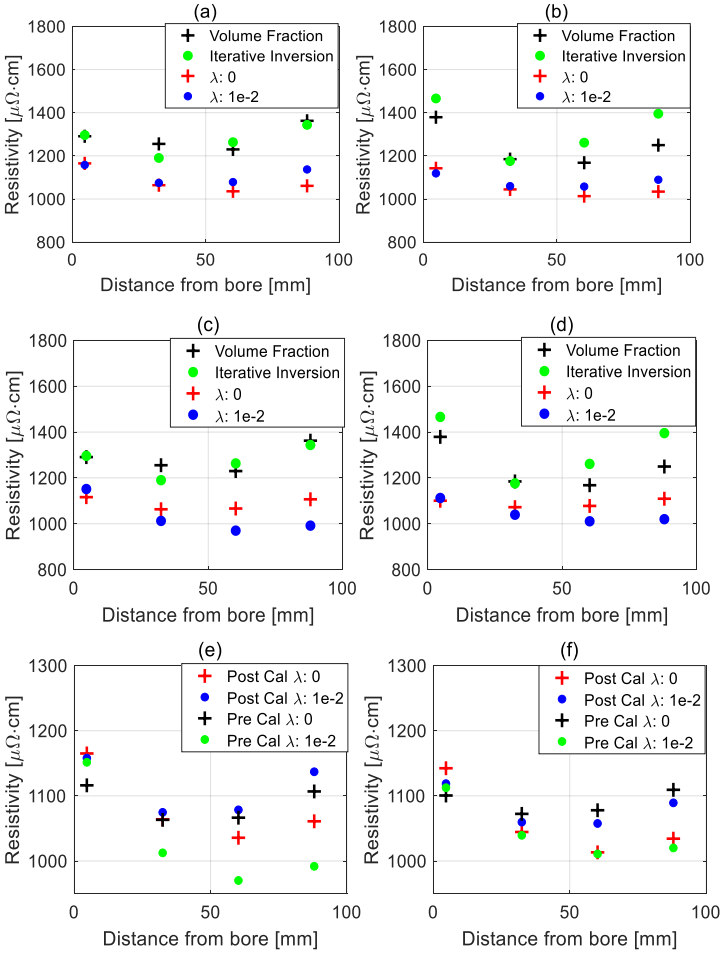

Fig. 11: Comparisons between selected profiles of the ANN from Fig. 8, iterative inversion and volume fraction calculations. (a) and (b) Profiles estimated using ANN with post-calibration data, (c) and (d) Profiles estimated using ANN with pre-calibration data (e) and (f) Profiles estimated using post-calibration data verses pre-calibration data. Note for comparison purpose the evaluation points on the x-axis is reduced to four points.

TABLE III

ERROR NORM BETWEEN THE ANN OUTPUT AND ITERATIVE INVERSION SOLUTION AGAINST VOLUME FRACTION MODEL ESTIMATE FOR PATTERN (A) AND (B) SHOWN IN FIG.11

ANN	Error norm w.r.t parallel model estimate	
Reg-pram	Pattern (a)	Pattern (b)
Post-Cal $\lambda = 0$	14.35 %	13.32 %
Post-Cal $\lambda = 10^{-2}$	11.82 %	13.94 %
Pre-Cal $\lambda = 0$	15.53%	13.75 %
Pre-Cal $\lambda = 10^{-2}$	20.72 %	16.49 %
Iterative	3.33 %	5.12 %

leading to less accurate solution. A comparisons between the estimated resistivity values from the ANN trained with $\lambda = 0$ and $\lambda = 10^{-2}$ before and after calibrating the test data, the volume fraction estimate and the solution from iterative inversion are also shown in Table II, Table III and Fig. 11. A detailed look into the estimated bore and periphery profiles in Table II and Fig. 11 reveals that the change between the bore and periphery resistivity profiles are proportional, but the resistivity profiles predicted using the volume fraction formula and iterative inversion tend to agree reasonably well and generally larger than the profiles estimated using the ANNs.

The resistivity values estimated using the calibrated data for pattern (a) between the bore and periphery (for the ANN trained with $\lambda = 0$ and $\lambda = 10^{-2}$) have $104\ \mu\Omega.\mathrm{cm}$ and $21\ \mu\Omega.\mathrm{cm}$ difference whereas values estimated using a data prior to calibration shows $9\ \mu\Omega.\mathrm{cm}$ and $160\ \mu\Omega.\mathrm{cm}$, both in a reversed direction relative to the hole spacing. In contrast the profiles estimated from iterative inversion shows $47\ \mu\Omega.\mathrm{cm}$ differences in the correct direction relative to the hole spacing. These suggest that the 2.95 mm difference in hole spacing between the bore and periphery was not captured by the ANN. This could be due to the reduced amount of training data used to produce the ANN for this particular laboratory sample, which in this case is 912 multi-frequency datasets compared to reactor brick ANN datasets (10583).

The error norms between the ANN outputs and iterative inversion solution against the predicted resistivity values from the volume fraction model (Fig. 11 (a) to 11 (f)) are shown in Table III. The results indicate that each of the ANN perform slightly better than one another when estimating the two profiles. However, when considering the accumulated mean error between the two ANN models, it can be clearly seen that the ANN trained with $\lambda = 10^{-2}$ perform better with calibrated test data and become less accurate when using un-calibrated test data. In contrast the ANN trained with $\lambda = 0$ perform better with uncalibrated data and vice versa. The reason we see these, particularly for the un-calibrated data may be due to the added errors into the training data, which allows the model to tolerate some amount of errors in the test data without having additional regularisation into the model. The solution from the iterative inversion clearly performs better than the two ANN models, however one of the drawbacks with iterative approach is that it lacks the speed that can be achieved from ANN models.

Fig. 13, 14 and 15 show the estimated profiles of reactor fuel channel bricks. The actual resistivity profiles for the reactor bricks at the location where the EC data collected was first assumed unknown. Therefore, as in the previous case we used two different criteria for selecting a suitable regularisation parameter in order to achieve an accurate solution. The first criteria was based on the results from the unseen datasets presented in Fig. 7 and Table I, which indicated that the smallest profile errors are achieved when the ANN is trained with $\lambda = 10^{-7}$and $\lambda = 10^{-5}$, whereas the second criteria is based on the estimated solution that gives the least error with respect to the homogeneous profile from the calibration brick.

Fig. 12 shows a plot of regularisation parameters verses profile errors with respect to the known bulk resistivity value of the calibration brick used during the reactor brick measurement. The results in Fig. 12 clearly indicated that the smallest profile error with respect to the homogenous resistivity profile is achieved when the ANN is trained with and $\lambda \leq 10^{-5}$ which is in accord with the results from unseen simulated data shown in Fig. 7 and Table I. As the values of λ increases beyond 10^{-5}, the error between the estimated and target profiles increased rapidly.

As previously mentioned, the training data for this particular study consists of various types of artificial errors replicating the physical measurements to allow for some level of error tolerance, and to generalise the network to unseen test

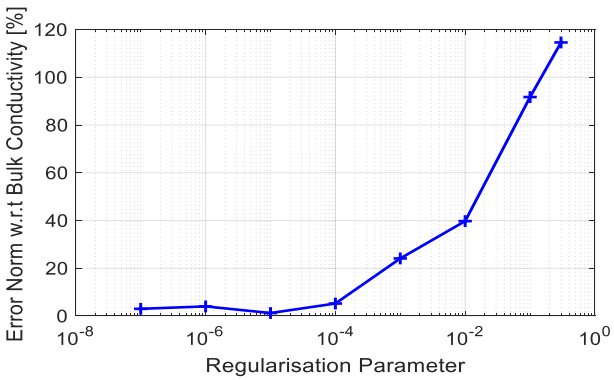

Fig. 12: Reactor brick ANN regularisation parameter verses profile errors with respect to the brick with known bulk conductivity

data. Therefore, the training data itself in this case could be considered as a form of regularisation to map the unseen input data to the predicted output. This is mainly due to the fact that the errors were only distributed on the input datasets while maintaining identical output datasets during the training procedure allowing for some levels of measurement error tolerance, and hence this could be the reasons why the ANN works best with small values of λ than larger values.

Comparison of selected regularisation parameters between the laboratory and the reactor brick shows significant difference. The reason that the regularisation parameter for laboratory brick ($\lambda = 10^{-2}$) is larger than the reactor brick ($\lambda \leq 10^{-5}$) could lie in the artificial errors added to the training dataset. Since the artificial errors are generated as $[D_{IN}\ \ (D_{IN} + \varepsilon)] \Rightarrow [D_T\ \ D_T]$ where D_{IN} is the original simulated error-free data, ε is the errors added on the original training datasets and D_T is the target datasets, the more original training datasets are available the highest the number of datasets with added artificial errors incorporated into training datasets and vice versa. This means that the more added error in the training dataset act as some form of regularisation. Therefore, due to the large amount of training datasets used to train the reactor brick ANN (10583 multi-frequency datasets) compared with the 912 multi-frequency datasets used for the laboratory brick ANN, it is reasonable to expect that the regularisation parameter that gives the least error for laboratory brick ANN to be larger than the ANN for the reactor brick.

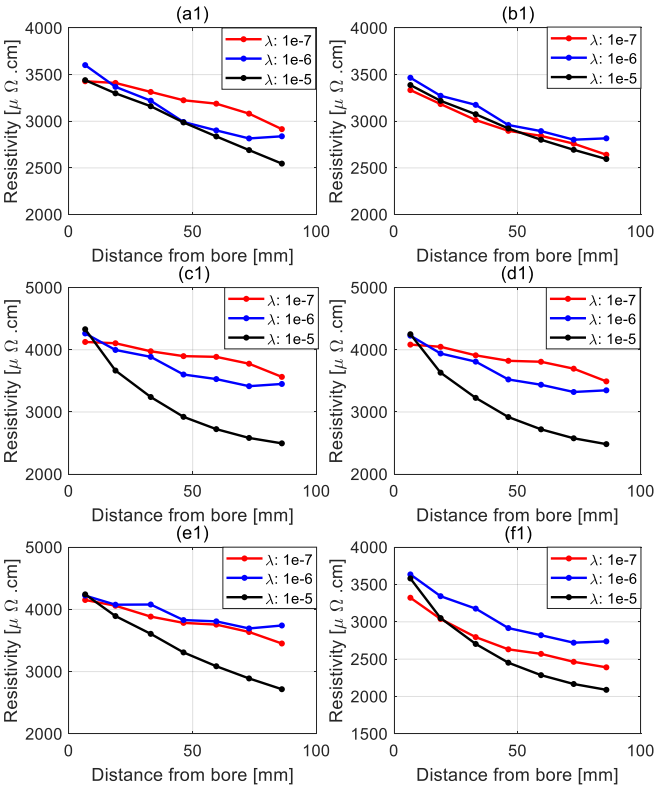

Fig.13: Estimated resistivity profiles of reactor brick using the measurement collected from one of the operating reactor core from channel X at the top of each brick.

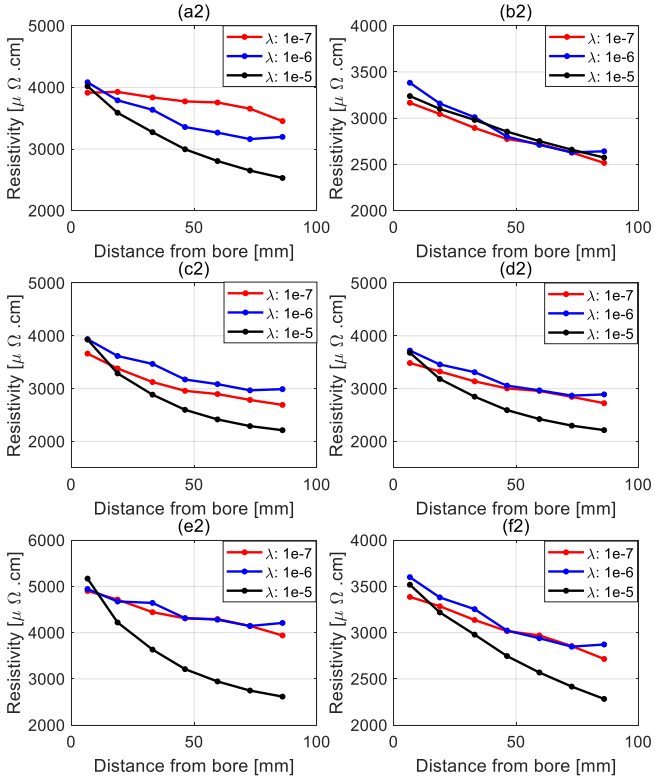

Fig.14: Estimated resistivity profiles of reactor brick using the measurement collected from one of the operating reactor core from channel X at the bottom of each brick.

The results in Fig.13, Fig. 14 and Fig. 15 show the resistivity profiles estimated using the measurements collected from one of operating reactor fuel channel at twelve different locations, (a1) to (f1) and (a2) to (f2). In Fig.13 and Fig. 14 each of the plots show three different curves of the estimated profiles from the ANNs trained with three different regularisation parameters, whereas Fig 15 shows the estimated profiles for the ANN trained with $\lambda = 10^{-5}$ and the iterative inverse solution along with the measurements of the trepanned sample taken out of the reactor core. The plots in Fig.13 and Fig. 14

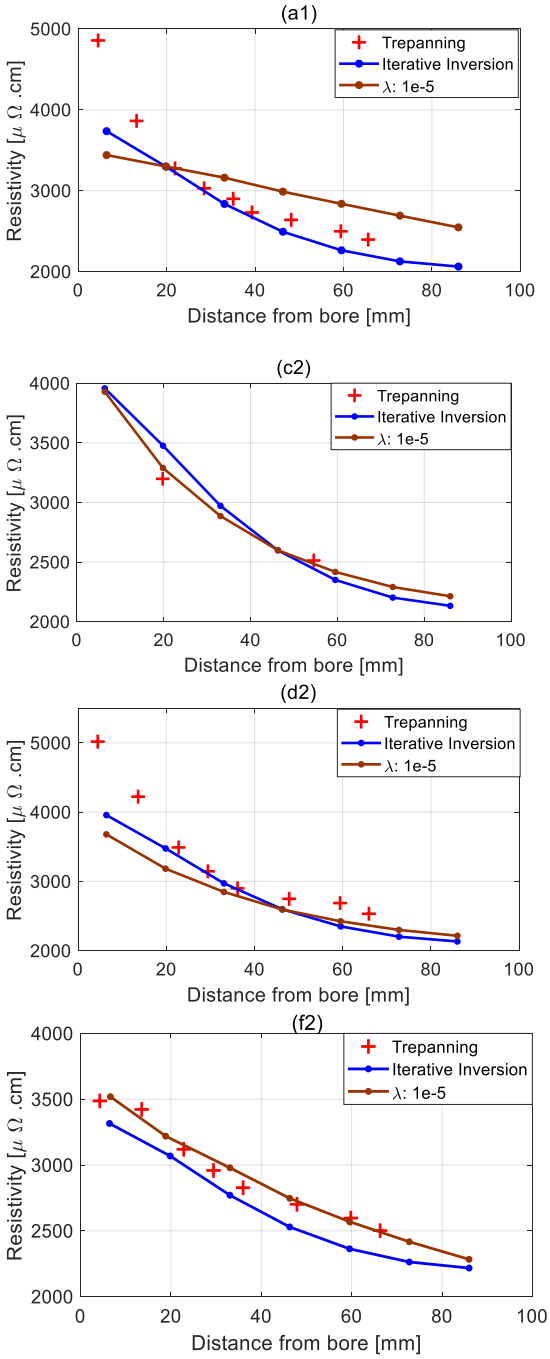

Fig. 15: Comparisons of the estimated profiles from the ANN and iterative inversion against the measurement collected from trepanned sample taken out of the reactor core.

TABLE IV
COMPARISONS BETWEEN THE MEAN ANN OUTPUTS AND ITERATIVE INVERSE SOLUTIONS AGAINST THE MEAN TREPANNED SAMPLE MEASUREMENTS

	Mean Profile Error	
	ANN ($\lambda = 10^{-5}$)	Iterative inversion
Position a1	4.40 %	14.20 %
Position c2	1.84 %	1.50 %
Position d2	17.80 %	16.90 %
Position f2	5.50 %	14.30 %

shows close estimate of the bore resistivity values for all three cases. However, as the distance from the bore increases the difference between the estimated profiles tend to increase. This suggest that the EC probe response to a change in graphite resistivity near the bore (the high frequency component of the inductance spectra) is much stronger than the low frequency component allowing the network to map the relationship between the input and the output accurately regardless of the tested regularisation parameter.

Comparison between the ANN output and the iterative inverse solution based on the algorithm in [21] against the trepanned sample measurements taken out of the reactor core at the locations where the EC measurements collected are shown in Fig. 15 and Table IV. The mean profile differences in Table IV indicates smaller difference between the ANN mean estimate and trepanning measurement for the positions a1 and f2. However, this type of comparisons gives only a partial insight into the performance of the selected approaches as a constant profile with some fixed value could also give much less mean difference than the profiles that shows the actual trend of the true profile. Nevertheless, the combinations of the profile plots in Fig. 15 and the profile differences in Table IV gives a complete picture of the performance between the two approaches. From these two results we can see that the ANN performs as good as the iterative inversion algorithm except for position a1, where the ANN output shows almost linear profile.

V. CONCLUSION

The use of machine learning and artificial neural networks within the non-destructive testing applications are still an emerging approach. One of the main advantages of this approach, particularly in the context of resistivity profiling from the eddy current measurement is that its speed compared with traditional iterative inversion algorithms, although the accuracy of the solution largely dependent up on the amount of training datasets covering multiple scenarios of the test condition. In this paper, we presented a method based on artificial neural network for estimating the reactor brick resistivity profiles as a function depth from multi-frequency eddy current measurements. A combination simulated data, laboratory measurements and the measurement collected from the one of operating reactor core were used to test the artificial neural network models. The estimated profiles from laboratory sample and the reactor measurements were compared against the solutions from the iterative inversion algorithm and showed reasonable agreement between one another suggesting that the artificial neural network could in principle perform as good as traditional iterative inversion algorithms provided sufficient datasets are used for training. Further comparison of the estimated profiles from the reactor measurements against the trepanned sample measurements taken out of the reactor core at the locations where the eddy current data is collected show a profile difference ranging between 1.84 % and 17.80 %.

ACKNOWLEDGMENTS

The authors would like to thank the UK Engineering and Physical Science Research Council and EDF Energy for funding this project under the EPSRC / University of Manchester grant number IAA 122.

REFERENCES

[1] A.G. Steer, "AGR Core Design, Operation and Safety Functions." Management of Ageing in Graphite Reactor Cores. Cambridge: Royal Society of Chemistry. ISBN: 0854043454, 2007, pp.11-18.

[2] B. T. Kelly, B. J. Marsden, K. Hall, D. G. Martin, A. Harper, and A. Blanchard. "Irradiation damage in graphite due to fast neutrons in fission and fusion systems." IAEA-TECDOC-1154, IAEA, Vienna, 2000.

[3] J. H. W. Simmons, "Radiation Damage in Graphite." International Series of Monographs in Nuclear Energy. Vol. 102. Amsterdam, The Netherlands: Elsevier, 2013.

[4] P.J. Hacker, G.B. Neighbour and B. McEnaney, "The coefficient of thermal expansion of nuclear graphite with increasing thermal oxidation." Journal of Physics D: Applied Physics, Vol. 33, no 8, pp 991-998, 2000.

[5] T. Bloodworth, M. Anderson, M. Brown and J. Williams, "Eddy current inspection of AGR fuel channels: keyway cracks and density mapping." In Proc. NDT, Northamptonshire, UK, 2012.

[6] J. García-Martín, J. Gómez-Gil, and E. Vázquez-Sánchez, "Non-destructive techniques based on eddy current testing." Sensors, Vol. 11, no. 3, pp. 2525-2565, 2011.

[7] H. Tesfalem, A. D. Fletcher, M. Brown, B. Chapman, and A. J. Peyton. "Study of asymmetric gradiometer sensor configurations for eddy current based non-destructive testing in an industrial environment." NDT & E International, Vol. 100, pp.1-10, 2018.

[8] S. J. Norton, A. H. Kahn, and M. L. Mester, "Reconstructing electrical conductivity profiles from variable-frequency eddy current measurements." Journal of Research in Nondestructive Evaluation, Vol. 1, no. 3, pp. 167-179, 1989.

[9] S. J. Norton, and J. R. Bowler, "Theory of eddy current inversion". Journal of Applied Physics, Vol. 73, no. 2, pp. 501-512, Jan. 1993

[10] J. R. Bowler and J. N. Stephen, "Eddy current inversion for layered conductors." Journal of Research in Non-destructive Evaluation" Vol. 4, no. 4, pp. 205-219, 1992.

[11] J. C. Moulder, E. Uzal, and J. H. Rose, "Thickness and conductivity of metallic layers from eddy current measurements." Review of scientific instruments, Vol. 63, no. 6, pp. 3455-3465, Jun. 1992.

[12] E. Uzal, J. C. Moulder, S. Mitra, and J. H. Rose, "Determining conductivity and thickness of continuously varying layers on metals using eddy currents." In Review of Progress in Quantitative Nondestructive Evaluation, Boston, MA, USA: Springer, pp. 251-258, 1993.

[13] W. Yin, S. J. Dickinson, and A. J. Peyton, "Imaging the continuous conductivity profile within layered metal structures using inductance spectroscopy." IEEE Sensors Journal, Vol. 5, no. 2, pp. 161-166, 2005.

[14] W. Yin, S. J. Dickinson, and A. J. Peyton, "Evaluating the permeability distribution of a layered conductor by inductance spectroscopy." IEEE transactions on magnetics, Vol. 42, no. 11, pp. 3645-3651, 2006.

[15] W. Yin, and A. J. Peyton, "Determining the Step-change Conductivity Profile within Layered Metal Structures Using Inductance Spectroscopy." IEEE Instrumentation and Measurement Technology Conference Proceedings, Dec 2006, pp. 2127-2131.

[16] C. V. Dodd. and W. E. Deeds. "Analytical solutions to eddy-current probe-coil problems." Journal of applied physics, 39(6), 2829-2838, 1968.

[17] B. Dekdouk, R. Chapman, M. Brown, and A. J. Peyton, "Evaluating the conductivity distribution in isotropic polycrystalline graphite using

spectroscopic eddy current technique for monitoring weight loss in advanced gas cooled reactors." NDT & E International, Vol. 51, pp. 150-159, Oct. 2012.
[18] A. D. Fletcher, "Non-destructive testing of the graphite core within an Advanced Gas-Cooled Reactor." Doctoral dissertation, The University of Manchester, Manchester, UK, 2014.
[19] H. Tesfalem, A. Peyton, A. Fletcher, M. Brown, and B. Chapman, "Eddy Current Sensors and Inversion Techniques for Estimation of the Conductivity Profile of the Graphite Bricks in an Advanced Gas-cooled Reactor Core". Vol. 42, Amsterdam, The Netherlands: IOS press, 2017, pp.253-264.
[20] H. Tesfalem, "Eddy Current Based Non-Destructive Testing of the Advanced Gas-Cooled Reactor Core." Doctoral dissertation, The University of Manchester, Manchester, UK, 2018.
[21] H. Tesfalem, A. J. Peyton, A. D. Fletcher, M. Brown and B. Chapman, "Conductivity Profiling of Graphite Moderator Bricks from Multi-Frequency Eddy Current Measurements," in IEEE Sensors Journal, Jan 2020, doi: 10.1109/JSEN.2020.2965201.
[22] N. Bowler and Y. Huang, "Electrical conductivity measurement of metal plates using broadband eddy-current and four-point methods," Measurement Science and Technology, Vol. 16, no. 11, pp. 2193–2200, Sep. 2005.
[23] Ma, X., and Peyton, A. J. "Eddy current measurement of the electrical conductivity and porosity of metal foams". IEEE Transactions on instrumentation and measurement, 55(2), 570-576, 2006.
[24] A, Tamburrino. and G, Rubinacci. "Fast methods for quantitative eddy-current tomography of conductive materials." IEEE transactions on magnetics, 42(8), 2017-2028, 2016.
[25] C. Liu, X. Han, Q. Chen, Z. Wu, D. Wei and J. Ren, "Non-contact electrical resistivity measuring system based on BP neural network," 2018 IEEE International Instrumentation and Measurement Technology Conference (I2MTC), 2018, pp. 1-6, doi: 10.1109/I2MTC.2018.8409680
[26] A. A Carvalho, J. M. A. Rebello, L. V. S. Sagrilo, C. S. Camerini, and I. V. J. Miranda, "MFL signals and artificial neural networks applied to detection and classification of pipe weld defects." NDT and E International, Vol. 39, no. 8, pp. 661-667, Dec. 2006.
[27] P. Zhu, Y. Cheng, P. Banerjee, A. Tamburrino, and Y. Deng, "A novel machine learning model for eddy current testing with uncertainty." NDT and E International, Vol. 101, pp. 104-112, Jan. 2019.
[28] V. S. Eremenko, A. V. Pereidenko, and E. F. Suslov, "Neural Network Based System for Nondestructive Testing of Composite Materials Using Low-Frequency Acoustic Methods." Universal Journal of Engineering Science, Vol. 1, no. 3, pp. 95-109, 2013.
[29] C. Wunderlich, C. Tschöpe, and F. Duckhorn, "Advanced methods in NDE using machine learning approaches." In AIP Conference Proceedings, Vol. 1949, no. 1, 020022. AIP Publishing, Apr. 2018, DOI: 10.1063/1.5031519.
[30] S. Lawrence, C. L. Giles and A. C. Tsoi, "Lessons in neural network training: Overfitting may be harder than expected." Proceedings of the fourth national conference on artificial intelligence, AAAI-97, Menlo park, California, pp. 540-545, Jul. 1997.
[31] J. Hampton, H. Tesfalem,, A. Fletcher, A. Peyton, M Brown "Reconstructing the conductivity profile of graphite block using inductance spectroscopy with data-driven techniques. The Britsh Institute of Non-Destructive Testing, Vol 63, pp 82-87, February 2021,
[32] G. D. Magoulas, and M. N. Vrahatis, "Adaptive algorithms for neural network supervised learning: a deterministic optimization approach." International Journal of Bifurcation and Chaos, Vol. 16, no. 7, pp. 1929-1950, Jul. 2006.
[33] K. J. Cios, and I Shin, "Image recognition neural network". Neurocomputing, Vol. 7, no. 2, pp. 159-185, Mar. 1995.
[34] D. De Ridder, R. P. Duin, M. Egmont-Petersen, L. J. Van Vliet, and P. W. Verbeek, "Nonlinear image processing using artificial neural networks." In advances in image and electron physics, Vol. 126, pp 351-450, Elsevier, Jan. 2003.
[35] Wunderlich, C., Tschöpe, C., & Duckhorn, F. "Advanced methods in NDE using machine learning approaches". In AIP Conference Proceedings, Vol. 1949, No. 1, p. 020022. AIP Publishing LLC, April 2018.
[36] Harley, J. B., & Sparkman, D. "Machine learning and NDE: Past, present, and future." In AIP Conference Proceedings (Vol. 2102, No. 1, p. 090001). AIP Publishing LLC, May 2019.
[37] Lorenzi, A. "Artificial Neural Networks Methods to Analysis of Ultrasonic Testing in Concrete. "In Fall Conference & Quality Testing Show 2012, pp. 257-265, October 2012.
[38] I. Giannakis, A. Giannopoulos, and C. Warren "A machine learning-based fast-forward solver for ground penetrating radar with application to full-waveform inversion." IEEE Transactions on Geoscience and Remote Sensing, Vol. 47, no. 7, pp. 4417-4426, Jan 2019.
[39] Wang, M., & Pan, N. Predictions of effective physical properties of complex multiphase materials. Materials Science and Engineering: R: Reports, Vol 63, no 1, pp 1-30, (2008).

HenokTesfalem received the M.Eng. degree in Electrical and Electronics engineering in 2014 and the Ph.D. degree in 2018 from the University of Manchester, Manchester, U.K. His Ph.D. thesis was titled "Eddy current based non-destructive testing of the graphite bricks in an advanced gas-cooled reactor core". He joined the University of Manchester as a post-doctoral research associate in April 2018. His research focuses in electromagnetic non-destructive testing including conductivity profiling and defect detection and characterization.

Joel Hampton received the B.Eng. degree in Electrical and Electronic engineering in 2018 from the University of Manchester, Manchester, U.K. He is currently in the third year of a Ph.D. project with the title "Electromagnetic non-destructive testing of the graphite core of advanced gas cooled reactors".

Adam D Fletcher received the MSci degree in Mathematics and Physics in 2008 from the University of Durham, UK and the EngD degree in Nuclear Engineering from the University of Manchester, UK in 2014. This PhD thesis was titled "Non-destructive Testing of the Graphite Core within an Advanced Gas-Cooled Reactor". He joined EDF Energy in 2014 as a Graphite Core Inspection Engineer implementing new techniques for AGR core inspection. He returned to Manchester University in 2019 as a Research Associate developing electromagnetic techniques for landmine detection. His main research interests are in electromagnetic non-destructive testing systems, sensor systems, inverse problems and computational electromagnetics.

Matthew Brown received a Ph.D. in Materials from UMIST, UK in 2002. His Ph.D. thesis was titled "Investigation of microwave plasma deposited silica coatings on carbon fibres used in aluminium matrix composites". He subsequently joined BNFL and worked at Berkeley Laboratory for four years on the characterisation of irradiated PGA graphite for Magnox reactors. He joined EDF-Energy in 2006 and has since worked on the development of graphite inspection techniques for AGR reactors.

Anthony J. Peyton received the B.Sc. degree in electrical and electronics engineering in 1983 and the Ph.D. degree in 1986 from the University of Manchester, Manchester, U.K. His Ph.D. thesis was titled "Device for the assessment and rehabilitation of kinetic muscle function and circuitry for monitoring localized muscle fatigue." He was appointed as Principal Engineer at Kratos Analytical Ltd. in 1989, developing precision electronic instrumentation systems for magnetic sector and quadrupole mass spectrometers, from which an interest in electromagnetic instrumentation developed. He returned to University of Manchester as a Lecturer and worked with the Process Tomography Group. He moved to Lancaster University in 1996, taking up post of Senior Lecturer. He was promoted to reader in Electronic Instrumentation in July 2001 and Professor in May 2004. Since December 2004, he has been Professor of Electromagnetic Tomography Engineering at The University of Manchester. His main research interests currently are in the area of instrumentation, applied sensor systems, and electromagnetics including non-destructive testing systems, ground penetrating radar systems, security scanning and landmine detection systems.